Abstract

A flare is an explosive phenomenon caused by the impulsive release of magnetic energy in the outer stellar atmosphere. While solar flares provide the most detailed view of magnetic energy release in astrophysical plasmas, observations of flares on other stars offer access to flares of much larger physical scales beyond what are attainable in the solar corona.

Giant flares from magnetically active stars, such as RS CVn-type binaries, generate high-temperature plasma of 10–100 MK, making X-ray spectroscopy essential for constraining their physical properties. In particular, the Fe K-shell transitions of highly charged ions provide sensitive diagnostics of both thermal and non-thermal plasma properties. However, previous X-ray observations had limitations in (i) agility for rapid follow-up of flares, (ii) effective area, and (iii) spectral resolution in the Fe K band (6–9 keV). Consequently, fundamental questions regarding the multi-thermal structure and chemical composition of the hottest plasma in flares, as well as possible signatures of non-equilibrium ionization (NEI) and non-Maxwellian electron distributions, have remained largely unexplored.

Recent X-ray missions have opened new observational windows. NICER and XRISM make significant improvements over the three limitations above. NICER provides high-throughput soft X-ray spectroscopy with a large dynamic range, enabling time-resolved studies of the flare evolution. In combination with MAXI, a rapid follow-up system for transient sources has been established. XRISM employs the microcalorimeter-based spectrometer *Resolve*, which delivers unprecedented spectral resolution in the Fe K band for astrophysical sources beyond the Sun.

To fully exploit observational data of these missions, reliable experimental benchmarks and physical models are required. Laboratory measurements using an Electron Beam Ion Trap (EBIT) and X-ray microcalorimeter offer controlled data sets about line formation and satellite-line behavior, while hydrodynamic simulation provides a theoretical framework for interpreting the observed results.

With all these advances in recent years, we aim to make a progress in our understanding of stellar coronae with the following three objectives:

1. Establishing Fe K diagnostics for X-ray microcalorimeter spectra of coronal plasma.
2. Investigating departures from thermal equilibrium during flares.
3. Investigating multi-thermal structure and elemental abundances.

To achieve these objectives, we studied five complementary topics across three methods as shown in Figure 1. The three methods are: (I) experiments, (II) observations, and (III) simulation. The topics are: (I) Laboratory experiment with EBIT, (IIa) the UX Ari flare observation with MAXI+NICER, (IIb) the GT Mus quiescence observation with XRISM, (IIc) the HR 1099 flare observation with XRISM, (III) Hydrodynamic simulation with HYDRAD. The results of each topic are summarized below.

I) EBIT experiment: Using the EBIT facility equipped with an X-ray microcalorimeter at the Lawrence Livermore National Laboratory, we measured X-ray line emission from highly charged Fe ions using an X-ray microcalorimeter. We adopted the EBIT energy-sweeping technique, which can simulate X-ray emission from arbitrary electron-energy distributions. Two measurements were made; one is the Maxwellian distribution

and the other is a non-Maxwellian distribution represented by the κ distribution with total exposure times of ∼0.48 Ms and ∼33 Ms, respectively. These yielded X-ray spectra with $\sim 10^3$ counts eV^{-1} around the Fe K region. The observed intensities of Fe XXIII–XXV Kα lines were compared with the major atomic codes (AtomDB, Chianti, and SPEX) and atomic structure calculations using FAC. The Maxwellian case exhibited overall consistency in the Fe XXIV–XXV lines, validating both the measurements and the analysis for these charge states. The non-Maxwellian case showed good agreement for the He-like Fe lines; however, line ratios involving different ionization stages did not agree so well, likely due to systematic uncertainties associated with the non-optimum Fe injection method. Importantly, although theoretical models predict increased uncertainties for extreme κ values (i.e., $\kappa \to 1.5$), the close agreement between the measured and predicted the He-like dielectronic recombination line (j) over the direct excitation line (w) ratio demonstrates that this diagnostic can be used with some reliability for XRISM data within the parameter range studied here.

IIa) UX Ari (flare) with MAXI+NICER: A giant X-ray flare from the RS CVn-type binary UX Ari was discovered with MAXI on 2020 August 17, followed by NICER observations 89 minutes later. NICER obtained 32 snapshot observations over one week, covering the entire flare including the rising phase. The flare reached an X-ray luminosity of 2×10^{33} erg s^{-1}, with a total released energy by radiation of $\sim 10^{38}$ erg in the 0.5–8.0 keV band. The NICER spectra were dominated by a hot continuum with Fe XXV Heα and Fe XXVI Lyα emission. The temperature peak preceded the flux peak, suggesting that NICER captured the period of plasma formation in the flaring loop. From the evolution of the continuum temperature, flux, and their time delay, we estimated a loop length of $\sim 3 \times 10^{11}$ cm and a peak electron density of $\sim 4 \times 10^{10}$ cm^{-3}. We also examined possible departures from collisional ionization equilibrium (CIE) using the Fe XXV/Fe XXVI resonance line ratio. The spectra were broadly consistent with CIE throughout the flare, though an ionizing plasma slightly out of equilibrium was not excluded during the rising phase.

IIb) GT Mus (quiescence) with XRISM: XRISM observed the RS CVn-type binary GT Mus during quiescence. For the first time in a stellar source, the main and satellite lines of the Fe XXIV–XXVI K-shell complexes were resolved. We performed line-ratio diagnostics to search for deviations from CIE and from a Maxwellian electron-energy distribution. Using five combinations of direct-excitation and dielectronic recombination satellite lines in the three line complexes (Fe Heα, Lyα, and Heβ), we found that the plasma is best described by a two-temperature thermal model with $kT \approx 1.7$ and 4.3 keV. This is consistent with the Fe XXV thermal broadening and with broadband spectral fits in the 1.7–10 keV range. Other forms of deviation, such as non-equilibrium ionization (NEI) or non-Maxwellian electron energy distribution, were not favored, which is reasonable for a quiescent stellar corona. Together with the EBIT measurements, this result demonstrates the utility of Fe K-shell line ratios with microcalorimeters for diagnosing coronal plasma conditions.

IIc) HR 1099 (flare) with XRISM: During a long (∼400 ks) XRISM calibration observation of the RS CVn-type binary HR 1099 (covering 1.5 binary orbits), a flare lasting ∼100 ks was detected by chance. Although not among the largest scale flares (the radiatively released energy of $\sim 10^{34}$ erg), it is the first stellar flare observed with a microcalorimeter spectrometer even including the Sun. The peak count rate was 6.4

times the quiescent level, clearly distinguishing the flare. Many emission lines were detected from 1.7–10 keV in both the flaring and quiescent phases. Using the high spectral resolution of XRISM in the Fe K band (6.5–7.0 keV), we resolved inner-shell transitions of Fe XIX–XXIV and outer-shell transitions of Fe XXV–XXVI. Because these ions peak at different temperatures, they enabled the construction of the differential emission measure (DEM) distribution from 1–10 keV (≈10–100 MK) using Fe lines alone, without assuming elemental abundances. The constructed DEM is bimodal, and only the hot component increased during the flare. Using this DEM, we derived elemental abundances and found significant enhancements during the flare only for Ca and Fe, which have the lowest first ionization potentials among the analyzed elements. No such increase was seen for Si, S, or Ar. This behavior resembles trends observed in some large solar flares and represents a clear stellar example of FIP-related abundance variations during flares.

III) 1D-HD calculation with HYDRAD: To aid the interpretations of these observational results, one-dimensional hydrodynamic simulations along a flare loop were conducted, covering the evolution from the initial energy injection to the post-flare cooling phase. We extended the HYDRAD code, widely used in solar studies, to the parameter regime far beyond solar flares. We investigated the following parameter spaces: loop lengths from 40 Mm to 1 Gm, flare heating rates from 0.1 to 10 erg cm^{-3} s^{-1}, and assumptions of CIE versus NEI by solving the rate equations along with the hydrodynamic equations. From these simulations, we derived scaling relations between observed parameters (apex temperature, X-ray light curve time scales, ionization timescale) and control parameters (loop length and heating rate). Using the derived scaling laws, we evaluate the UX Ari flare case. We find that the possible signature of ionizing plasma discussed in II) is more naturally explained by a CIE interpretation, based on the ionization timescale estimated from the simulations.

The results obtained in these five topics contribute to establish a framework for investigating giant stellar flares using high-resolution Fe K-shell spectroscopy, laboratory plasma benchmarks, and hydrodynamic modeling. Through these efforts, this dissertation (1) establishes a Fe K-shell diagnostic scheme optimized for X-ray microcalorimeter spectra, from laboratory measurements with EBIT to its application to XRISM data, (2) discusses the systematic constraints on NEI process in time-resolved NICER data using numerical simulations, and (3) reveals the multi-thermal structure and abundance evolution of the hottest flare component using XRISM as well as the simulation. These results demonstrate the scientific potential of microcalorimeter-based X-ray spectroscopy for stellar astrophysics and highlight the value of integrating laboratory measurements and numerical modeling with astrophysical observations. The advances presented here lay essential groundwork for future observations with XRISM and next-generation microcalorimeter observatories.

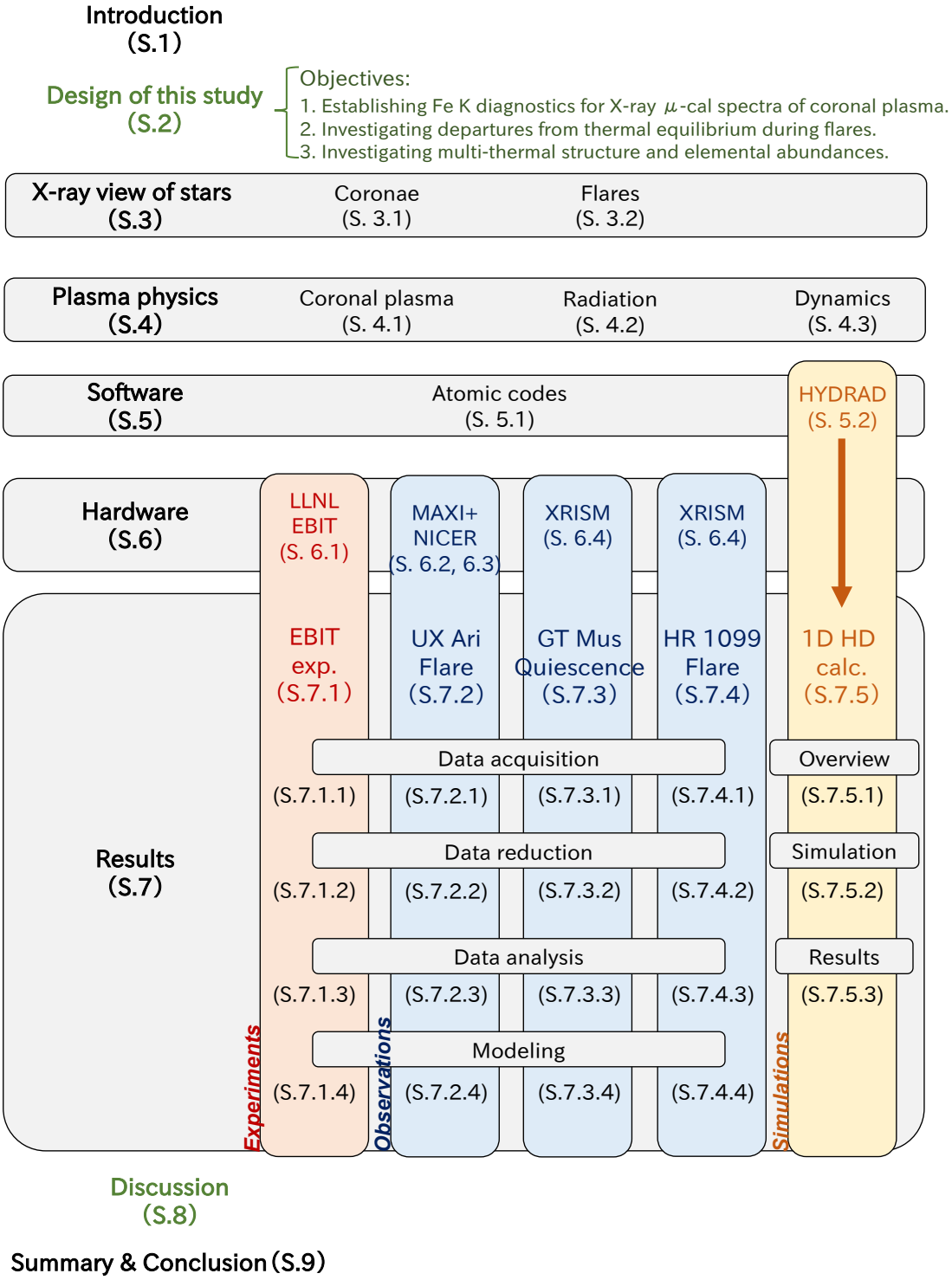

Figure 1: Structure of this dissertation